

In Situ QXAFS Study of the Pyrolytic Decomposition of Nickel Formate Dihydrate

A. Bryan Edwards[†] and C. David Garner

Department of Chemistry, University of Manchester, Manchester M13 9PL, U.K.

Kevin J. Roberts*

Centre for Molecular and Interface Engineering, Department of Mechanical and Chemical Engineering, Heriot-Watt University, Edinburgh, EH14 4AS, U.K., and CCLRC Daresbury Laboratory, Warrington WA4 4AD, U.K.

Received: May 22, 1996; In Final Form: September 25, 1996[⊗]

Quick scanning X-ray absorption fine structure (QXAFS) spectroscopy is applied to an examination of the pyrolytic decomposition of nickel formate dihydrate. Experimental QXAFS data reveal good quality edge and extended XAFS spectra being obtained in ca. 4 and 30 s, respectively. Comparison of data with normal (step/count) techniques reveals no adverse effect on the structural parameters derived using quick scanning. Temperature-programmed and isothermal decomposition studies are consistent with a pyrolysis mechanism involving rapid initial dehydration of the dihydrate followed by subsequent decomposition of the anion, via a nickel oxide intermediate, to yield a finely divided nickel metal (mean particle diameter ca. 12 Å). These data confirm the nature of the principle intermediate and final product, both previously uncertain.

Introduction

X-ray absorption fine structure (XAFS) spectroscopy is a sensitive probe of local atomic environment in condensed materials yielding information from the extended fine structure (EXAFS) on the type, number, and distance to the atoms surrounding the absorbing atom¹ as well as information from the near-edge structure (XANES) on the site symmetry and valence state of the absorber.² The technique is element specific, averaging over all atoms of a particular type. It does not depend on the presence of long-range order and can be applied to samples regardless of their physical state.

Despite the fact that the inherent time scale of XAFS is essentially that of electronic spectroscopy (ca. 10^{-15} s³), experimental considerations have generally limited its application to static systems because of the time required to collect data of sufficiently high quality to allow quantitative analysis. The normal mode of data collection employs a double-crystal monochromator to select a single wavelength from a broad spectrum source, usually synchrotron radiation with the spectrum being constructed from the collection of discrete measurements recorded at appropriate intervals over the desired energy range. A number of methods have been employed to extend XAFS to the time domain including freeze-quench techniques⁴ and time-resolved laser flash photolysis.⁵ A recent method is quick scanning XAFS, or QXAFS,⁶ in which the monochromator is swept across an angular range in a continuous movement and data collected by time-integrating absorption measurements recorded while the monochromator remains in motion. This approach reduces the energy resolution, since the measurements are no longer made at a single wavelength. However, by the choice of an appropriately short integration time relative to the speed of the monochromator, this can be maintained within acceptable limits. The energy resolution for EXAFS and XANES is ca. 5 and 1 eV, respectively.⁷ For a given monochromator speed the integration time will determine not only the energy resolution but also the sampling rate and signal-

to-noise ratio. It is therefore important that a suitable counting regime be established, the mechanics of the monochromator assembly having been shown to limit the time required to achieve high-quality data.⁸ In this paper we demonstrate the applicability of QXAFS to the structural characterization of nickel formate dihydrate, Ni(COOH)₂·2H₂O, and its subsequent pyrolytic decomposition through temperature-programmed and isothermal decomposition experiments. The measurements are validated, in a quantitative manner, via a comparison of normal and QXAFS mode data.

Experimental Details

Materials and Measurements. XAFS data were recorded on station 7.1 of the Daresbury synchrotron radiation source (SRS) operating in multibunch mode with a beam energy of 2 GeV and average circulating current of 170 mA. Data were collected in transmission mode using gas-filled ionization chambers and a Si(111) order sorting double-crystal monochromator. Reference data were collected between 300 eV below and $k = 15 \text{ \AA}^{-1}$ above the Ni K-edge with the monochromator detuned to 50% transmission to achieve a suitable level of harmonic rejection. The postedge data were collected at energies corresponding to increments of 0.04 in k -space with k^2 time weighting and final point integration time of 8000 ms.

QXAFS measurements, made using the FLYPAST option available within the Daresbury TOPOGRAPHY data acquisition program,⁹ were collected over a range of monochromator scanning speeds and data integration times in order to define optimal data acquisition conditions. A monochromator angle-scanning range 14 250–12 587 mdeg, corresponding to an energy range approximately equivalent to that used for the conventional step/count mode, was used with the monochromator detuned to about 40% transmission at the midpoint of the EXAFS region during data collection. The data were truncated at $k = 12 \text{ \AA}^{-1}$ prior to analysis owing to the existence of a reproducible discontinuity in the spectra when the monochromator was operated in QXAFS mode.

[†] Now at LSU College of Higher Education, The Avenue, Southampton SO9 5HB, U.K.

[⊗] Abstract published in *Advance ACS Abstracts*, November 15, 1996.

The nickel metal reference spectrum was recorded from a 5 μm rolled metal foil measuring some 4 cm \times 4 cm. Other data were recorded from AnalaR grade samples, ground into a fine powder and evenly diluted with boron nitride before being pressed into cylindrical pellets 10 mm in diameter and typically 1–2 mm thick in a high-pressure hydraulic press. Only those with an absorption step of 0.8–1.5 at the Ni K-edge were retained. These pellets were secured in a specially constructed electrically heated microfurnace¹⁰ for data acquisition. The temperature was measured using a previously calibrated thermocouple and quoted with an estimated error not exceeding ± 0.2 $^{\circ}\text{C}$.

The thermal behavior of nickel formate dihydrate was recorded using a DuPont 9900 differential scanning calorimeter from 6 mg of fresh nickel formate dihydrate in a sealed aluminum sample ampule heated at a constant rate of 2 $^{\circ}\text{C}$ min^{-1} .

Data Reduction and Analysis. Calibration and background subtraction of the raw absorption data were performed using unmodified versions of the Daresbury Laboratory programs EXCALIB and EXBACK, respectively. The isolated EXAFS data were analyzed within the framework of the curved wave theory¹¹ using the program EXCURV92.¹² Multiple scattering¹³ from collinear atomic arrangements was included in all simulations where appropriate. Phase shifts were derived from ab initio calculations using Hedin–Lundqvist exchange potentials and von Barth and Hedin ground states¹⁴ taken within a 1s core hole excited-state approximation. During analysis, the bond lengths (R), coordination numbers (N), and Debye–Waller-like disorder (2σ) were optimized using curve-fitting techniques in which the difference between the experimental and simulated spectra was minimized. However, the shell occupation number and disorder parameters, being highly correlated, typically prevented the coordination number from being determined to a precision better than ± 1 . The error in the bond length is estimated to be of the order of ± 0.03 \AA for the nearest-neighbor shell.

Results and Discussion

Validation of the QXAFS Implementation against Conventional Step/Counting Data Acquisition. The X-ray absorption spectrum of Ni metal was recorded at ambient temperature in QXAFS mode using a fixed integration time of 0.01 s at a variety of monochromator speeds. A comparison of the calibrated and normalized pre-edge and XANES absorption profiles with reference data recorded in normal mode (Figure 1) reveals that the resolution is insufficient, even at the highest sampling rate, to resolve the splitting in the first postedge feature. The pre-edge feature is similarly poorly reproduced in the QXAFS data with increasing monochromator speeds.

The energy dependent sampling frequency evident in the isolated EXAFS data (Figure 2) is due to the nonlinear relationship between the monochromator angle and photoelectron wave vector (k), the measurements having been made at equal time intervals with a monochromator moving with constant angular velocity. The trend in both energy resolution and counting statistics is unavoidable given the unsophisticated nature of this implementation. An inevitable consequence is to discriminate against accurate curve fitting of the contribution from low- Z neighbors whose scattering amplitude decreases more rapidly with increasing energy than heavy atom scatterers, concentrating the contribution low- Z neighbors make to the total EXAFS signal in the low k region. Similarly, the fitting of low- rather than high-temperature data is favored because of

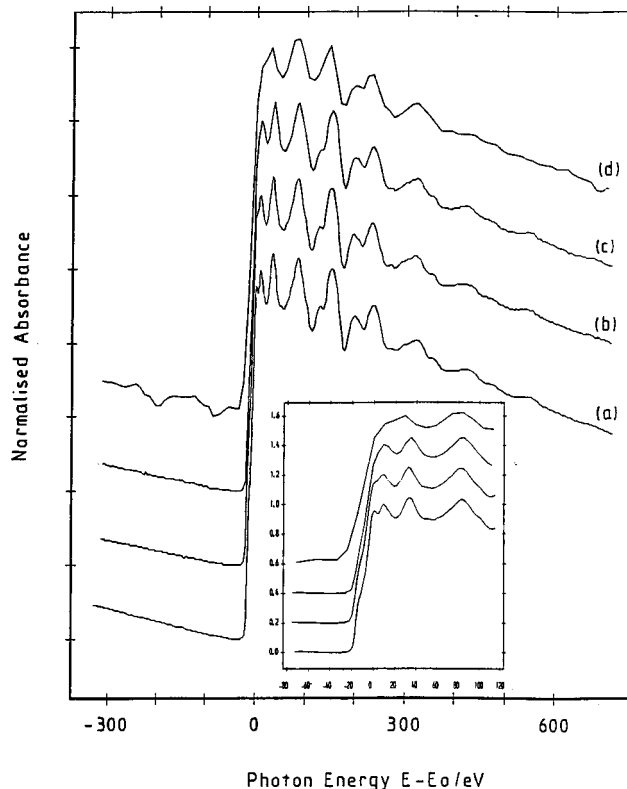


Figure 1. Comparison of K-edge X-ray absorption profiles for nickel metal recorded in normal step/count (a) and QXAFS (b–d) modes, the latter recorded with a constant integration time of 0.01 s and monochromator speeds of 20 mdeg s^{-1} (b), 50 mdeg s^{-1} (c), and 100 mdeg s^{-1} (d). The inset shows an expanded view of the pre-edge and XANES profiles of the same data.

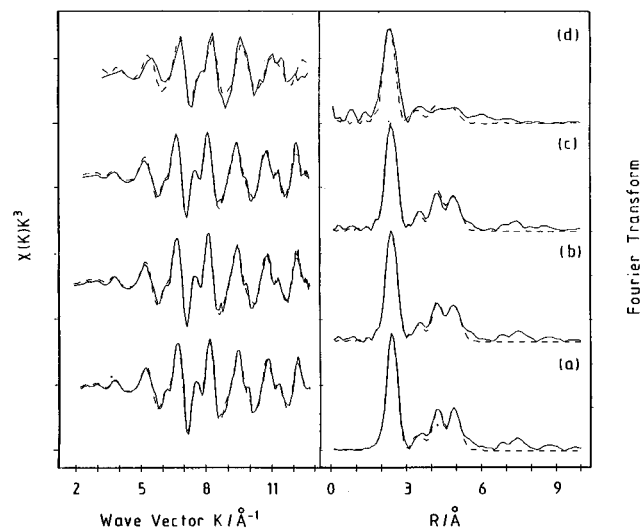


Figure 2. Comparison of isolated k^3 -weighted Ni-edge QXAFS data of nickel foil recorded at room temperature in normal step/count (a) and QXAFS (b–d) modes (—) and their associated Fourier transforms together with simulations based on the parameters listed in Table 1 (---). The QXAFS data were recorded with a constant integration time of 0.01 s and monochromator speeds of 20 mdeg s^{-1} (b), 50 mdeg s^{-1} (c), and 100 mdeg s^{-1} (d).

the damping effect of increased thermal disorder. Furthermore, relatively infrequent sampling of the low k data makes quantification of multiple scattering and other secondary processes unreliable and exaggerates the need for reliable phase shifts, which may differ considerably in this region depending on the computational methodology.

The similarity of the higher energy EXAFS data used for

quantitative analysis (i.e., beyond $k \approx 2.5 \text{ \AA}^{-1}$) was found to be generally good up to 50 mdeg s^{-1} . The effect of the systematic degradation in data quality with increasing monochromator speeds was evident in the Fourier transforms of these data. The most obvious manifestation is the failure to convincingly reproduce shells beyond the second in the fastest scan. A similar, though less dramatic, change can be seen in the more distant shells (beyond ca. 6.5 \AA) on moving from 20 to 50 mdeg s^{-1} , although in this case the differences occur beyond the maximum range normally included in quantitative analysis.

The total EXAFS above an absorption edge is the sum of damped sinusoidal contributions, one from each shell of atoms surrounding the absorber. The frequency of each contribution is proportional to the mean absorber–scatterer distance within that shell. Sampling theory dictates that such a sine wave must be sampled at a minimum of two points per cycle (i.e., twice the frequency of the wave) and a complex function at twice the frequency of the highest frequency component if it is to be accurately characterized by discrete sampling. This is commonly called the Nyquist condition.¹⁵ Thus, the sampling rate imposes a limit on the highest frequency of contribution that can be reliably isolated and, in turn, the maximum distance from the absorbed that can be probed. Increasing the monochromator scan speed without decreasing the integration time reduces the sampling rate to the extent that it fails to satisfy the Nyquist condition for ever closer shells as the monochromator speed increases. This could in principle be accommodated by reducing the integration time, since this would increase both the number of data points and their energy resolution. However, to do so would incur a penalty of poor counting statistics. The increasing dissimilarity between the QXAFS and reference data with increasing monochromator speed is attributed to sampling effects and demonstrates the need to validate an experimental regime against a previously characterized system before its application to an unknown.

Quantitative analysis of the data was performed by simulating scattering from the four nearest-neighbor shells. The shell occupation numbers and distances were initially set at the crystallographic values. The distances and their associated Debye–Waller parameters (which includes both structural and thermal disorder) and energy correction terms were subsequently refined. Multiple scattering from the collinear first and fourth shells was included (the scattering angle set to 180° and not refined during the fitting process). The optimized parameters (Table 1) confirm the observed qualitative agreement between the QXAFS and normal mode data. Despite the very significant reduction in data collection times, derived parameters for each of the four shells are identical within experimental error to the reference data for all but the fastest (100 mdeg s^{-1}) scan.

QXAFS Examination of the Decomposition Dynamics of Nickel Formate Dihydrate. There has been significant interest in the thermal decomposition of transition metal carboxylates as potential sources of high surface area solids for catalysis, which demands particles in the range $10\text{--}30 \text{ \AA}$ for maximum efficiency¹⁶ and whose properties are strongly size dependent in this range.¹⁷ More recently, there has been a resurgence of interest in microclusters with the discovery of a shell structure, similar to that of an individual atom or nucleus, dependent upon the number of atoms present.¹⁸ The pyrolysis of nickel formate and related carboxylates has been explored under a wide range of conditions using a variety of techniques for both bulk samples^{19–23} and well-defined surfaces.^{24–38} Collectively, these have aided an understanding of the factors affecting such reactions, although there are significant qualitative and quantitative differences reported for the mechanisms and energetics.

TABLE 1: Optimized Parameters Derived from Simulation of Ni K-Edge EXAFS of Nickel Foil Recorded in Normal and QXAFS Modes at Ambient Temperature^a

In Normal Mode						
shell	type	<i>N</i>	<i>R</i> (Å)	2σ (Å ²)	scan time (min:s)	
1	Ni	12	2.47	0.010	32:15	
2	Ni	6	3.49	0.017		
3	Ni	24	4.31	0.016		
4	Ni	12	4.95	0.014		
In QXAS Mode						
monochromator speed (mdeg s ⁻¹)	shell	type	<i>N</i>	<i>R</i> (Å)	2σ (Å ²)	scan time (min:s)
20	1	Ni	12	2.47	0.010	01:23
	2	Ni	6	3.49	0.017	
	3	Ni	24	4.32	0.017	
	4	Ni	12	4.97	0.015	
50	1	Ni	12	2.47	0.010	00:33
	2	Ni	6	3.50	0.017	
	3	Ni	24	4.32	0.016	
	4	Ni	12	4.97	0.015	
100	1	Ni	12	2.43	0.013	00:16
	2	Ni	6	3.42	0.017	
	3	Ni	24	4.27	0.026	
	4	Ni	12	4.89	0.024	

^a The shell occupation number (*N*) has been fixed at crystallographic value.

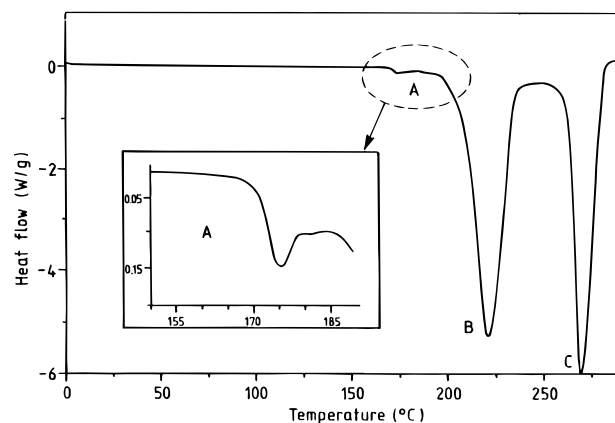


Figure 3. Differential scanning calorimetry trace for $\text{Ni}(\text{COOH})_2 \cdot 2\text{H}_2\text{O}$ in a sealed ampule. The data reveal three main regions: (A) dehydration, (B) conversion from anhydrate to oxide, and (C) reduction of oxide to metal. The inset shows an enlargement of region A.

Relatively few generalizations regarding points of similarity or trends within these comparable systems have been accorded widespread acceptance.

Temperature-Programmed Study. Differential scanning calorimetry (DSC) of nickel formate dihydrate (Figure 3) provides evidence of changes at ca. 175, 225, and $270 \text{ }^\circ\text{C}$ with no evidence for further changes to $350 \text{ }^\circ\text{C}$. A sample of nickel formate dihydrate was heated from ambient temperature to $310 \text{ }^\circ\text{C}$, without interruption, at a constant rate of $10 \text{ }^\circ\text{C min}^{-1}$. Absorption spectra were recorded at $30 \text{ }^\circ\text{C}$ steps to $180 \text{ }^\circ\text{C}$, then at $240 \text{ }^\circ\text{C}$ and finally at $310 \text{ }^\circ\text{C}$. The pyrolysis products were immediately cooled to room temperature and the absorption spectrum rerecorded.

The XANES (Figure 4) and EXAFS data (Figure 5) recorded in the temperature step experiment suggest negligible differences in the nickel coordination environment to $180 \text{ }^\circ\text{C}$, confirmed by the Fourier transforms of the EXAFS data. Further heating to $240 \text{ }^\circ\text{C}$ precipitates only a slight change in the feature at $k \approx 6 \text{ \AA}^{-1}$ and slightly greater than expected drop in the magnitude of the feature at $R \approx 4 \text{ \AA}$ based on the trend established at

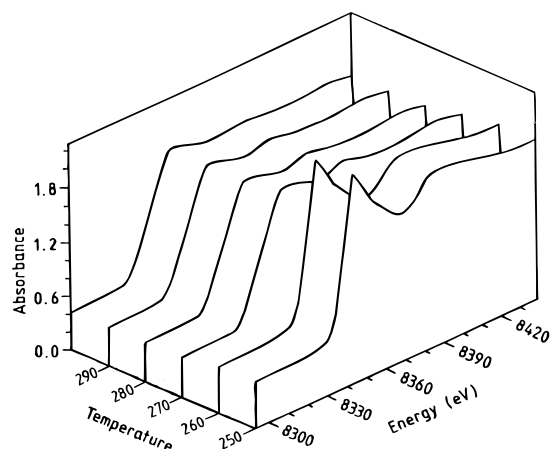


Figure 4. Temperature-programmed QXAFS data (XANES region) in the temperature region between 250 and 300 °C recorded with a data acquisition time of ca. 4 s, revealing a reduction of white line intensity associated with the thermally induced reduction of NiO to metallic Ni at around 265 °C.

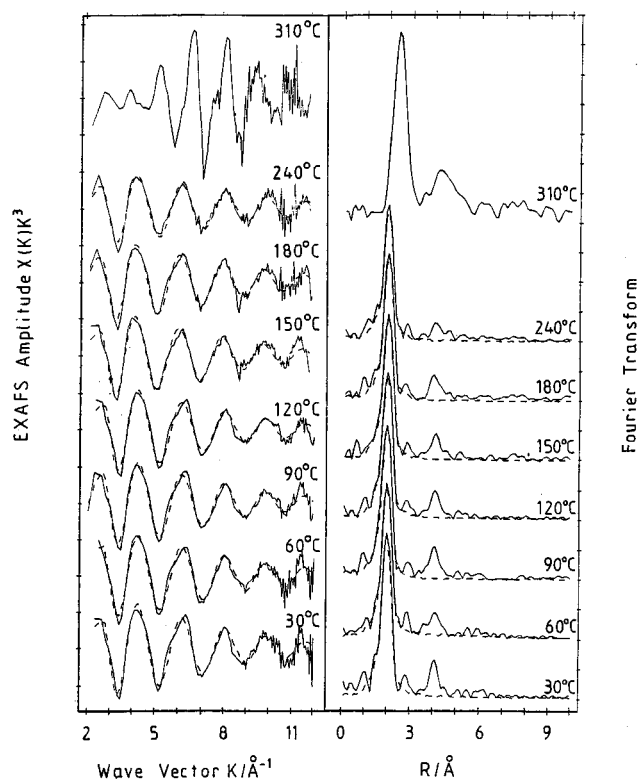


Figure 5. In situ temperature-programmed temperature dependent k^3 -weighted EXAFS data recorded in QXAFS mode with a fixed integration time of 0.01 s and monochromator speed of 20 mdeg s^{-1} (—) and associated Fourier transforms together with simulations based on the parameters listed in Table 2 (---).

lower temperatures. The data recorded at 310 °C are quite unlike that preceding it. Qualitatively similar to that of bulk metal, particularly at low k and R , the relative and absolute magnitudes of each Fourier transform feature are unlike those of the model system.

To avoid over parametrization of the simulation, the isolated EXAFS data to 240 °C were simulated assuming a single shell of oxygen backscatterers whose distance was initially set to 2 Å. Each of the structural parameters was allowed to float during the optimization, the amplitude being fitted by simultaneous refinement of both the shell occupation number and the Debye–Waller parameter. The optimized parameters (Table 2) support the view that the local atomic environment remains essentially

TABLE 2: Optimized Parameters Derived from Simulation of QXAFS Data from the Temperature-Programmed Decomposition Experiments

temperature (°C)	type	N	R (Å)	2σ (Å ²)
30	O	5.6	2.04	0.015
60	O	5.1	2.04	0.013
90	O	5.1	2.04	0.014
120	O	5.0	2.04	0.015
150	O	4.9	2.04	0.014
180	O	4.5	2.04	0.012
240	O	3.9	2.02	0.012

constant below 180 °C above which there is evidence of decreasing nearest-neighbor shell occupation.

Crystallographically characterized formate species are rare, making a direct comparison of the EXAFS-derived results difficult. However, a number of analogous covalently coordinated structural comparators do exist, e.g., *catena*-(tetraaquatetrakis(μ_2 -formato-O,O')dinickel(II))³⁹ has two distorted octahedrally coordinated nickel sites with a mean Ni–O distance of 2.063 Å. This is similar to the local atomic environment about nickel in diaquabis(acetylacetonato)nickel(II)⁴⁰ and bis(acetylacetonato)nickel(II) bis(ethanol)⁴¹ with mean Ni–O distances of 2.058 and 2.054 Å, respectively. In contrast, the 4-fold coordination of bis(2-hydroxy-5-methylacetophenato)nickel(II)⁴² has a reduced mean Ni–O distance of 1.84 Å. The structural parameters derived for nickel formate dihydrate at 30 °C (5.6 oxygen atoms at a mean distance of 2.04 Å) are thus chemically reasonable.

The DSC data, given in Figure 3, accords with a previous comparison of hydrated and anhydrous nickel formate salts,²³ with only the high-temperature feature common to both (the lower two absent in the anhydrous sample). Both EXAFS and DSC data are consistent with the first stage in the thermal decomposition of nickel formate dihydrate being elimination of water to yield anhydrous nickel formate. Changes in Ni–O distance are on the order of the statistical error associated with determination of this parameter and cannot be interpreted as definitive evidence of contraction of the primary coordination sphere with decreasing occupation, although they would be consistent with it. Indeed, the possible intermediate status of the anhydrous salt and the larger bond length of the Ni–O contact of nickel oxide (akin to that of the hydrated salt) into which it is converted (discussed subsequently) conspire against its identification by EXAFS, which yields data averaged over all atoms of a particular type. Dehydration could account for the reduction in $R \approx 4$ Å peak at 240 °C (Figure 5) by reducing any multiple scattering enhancement of the contribution from these more distant atoms by removing an intermediate oxygen atom. However, lattice reorganization to yield a new crystalline phase or amorphous material following initial dehydration prior to anion decomposition, observed in similar systems,⁴³ cannot be excluded on the basis of these data alone and for which there is limited evidence in the case of nickel formate dihydrate.²⁰ Although impossible to define the precise onset of dehydration, these data suggest that the hydrated phase persists to higher temperatures than sometimes reported, the onset of dehydration having been reported to be as low as 40 °C in vacuum.²⁰

Analysis of Decomposition Products. The data recorded from the cooled decomposition products were modeled as nickel metal assuming retention of the FCC structure. The bond lengths and disorder parameters for all four shells used in the simulation were initially set to those of the bulk metal. Scattering amplitudes were initially adjusted by varying the shell occupation numbers with simultaneous refinement of the interatomic scattering path lengths. The constant Debye–Waller constraint was subsequently relaxed and all parameters refined

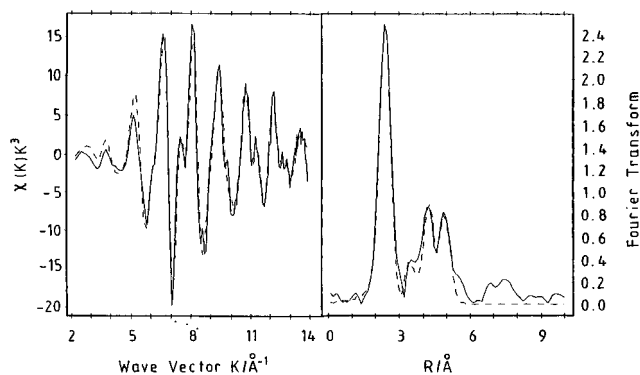


Figure 6. k^3 -weighted EXAFS data of the decomposition products as recorded in QXAFS mode with a fixed integration time of 0.01 s and monochromator speed of 20 mdeg s^{-1} (—) and associated Fourier transforms together with simulations based on the parameters listed in Table 3 (---).

TABLE 3: Optimized Parameters Derived from Simulation of QXAFS Data Recorded from the Decomposition Products Following Cooling Back to Ambient Temperature

shell	type	N	R (Å)	2σ (Å ²)
1	Ni	8.2	2.47	0.014
2	Ni	3.7	3.50	0.019
3	Ni	11.9	4.31	0.016
4	Ni	5.0	4.96	0.014

simultaneously. The best simulation and optimized parameters are presented in Figure 6 and Table 3, respectively. The refined parameters with those of the bulk FCC Ni (Table 1) reveals reduced coordination numbers for the reaction product associated with a particle size diameter (Table 4) of ca. 12 Å. Some caution is needed in directly comparing this with other measurements, since it is known that particle size estimation based on EXAFS coordination numbers can tend to slightly underestimate the particle size^{44–46} owing to the generation of asymmetric pair distribution functions by the very anharmonic motion of the atoms^{47,48} at even modest temperatures. Previously reported size estimates for this material range from 200 to 500 Å from electron microscopy²¹ to ca. 190 Å using X-ray diffraction²² and the integral breadth method.⁴⁹ However, direct comparison of the particle size with previous work is not very realistic, since the reaction is very sensitive to sample preparation and conditions that are not well documented in the literature. Our smaller particle size is probably consistent with temperature cycling rather than with products being maintained at elevated temperatures as in the other experiments.

Isothermal Study. A fresh nickel formate dihydrate sample with no prior thermal history was subsequently loaded into the furnace and the temperature raised as rapidly as possible to 180 °C and stabilized. Absorption spectra were recorded in QXAFS mode at regular intervals. Attempts to repeat the isothermal experiment at higher temperatures corresponding to onset of the transition at 270 °C were unsuccessful, the reaction being

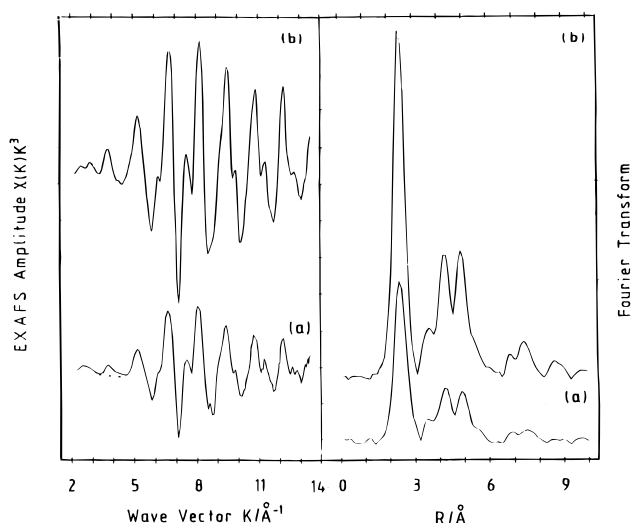


Figure 7. k^3 -weighted QXAFS data, together with associated Fourier transforms, showing a comparison between the pyrolyzed material produced in the temperature-programmed experiment (a) and data recorded from a reference nickel foil (b). Particle size estimates based on the analyzed data of the decomposed material, given in Table 3, are given in Table 4.

effectively instantaneous on the experimental time scale accessible using the current implementation.

The isolated, k^3 -weighted isothermal EXAFS data and their Fourier transforms (Figure 8) are suggestive of continuous change in the Ni environment over the time scale of the experiment. This is particularly apparent in the Fourier transforms with a reduction in the height of the nearest-neighbor shell accompanied by the emergence of a strong scattering from a shell centered at $R \approx 3$ Å. The data were analyzed using a simple two-shell model: a nearest-neighbor shell of oxygen atoms and more distant shell of Ni atoms at ca. 2 and 3 Å, respectively. The fitting procedure followed that outlined previously. The nickel shell was excluded from the simulation if it failed to offer a statistically significant improvement to the fit.⁵¹ The model, although simple, reproduces the principle features of the EXAFS and their Fourier transforms. The optimized results, collated in Table 5, suggest the creation of an oxide phase, the observed metal–metal distance of ca. 2.98 Å comparing favorably with the crystallographic distance of 2.954 Å.⁵² Other identifiable Ni–Ni contacts whose distances are consistent with those expected for NiO reinforce this assignment but were excluded from the final fit because of the high $\{\sigma, N\}$ correlation, making meaningful amplitude quantification impossible. The derived structural parameters are incompatible with a NiCO₃ intermediate proposed elsewhere.⁵³ This oxide intermediate is presumably reduced on further heating by CO, H₂ (both of which have been detected experimentally³⁸), and possibly other reactive intermediates generated in the course of the reaction but inhibited from diffusing from the reaction zone. It is probable that behavior in this region is ill-suited to description by balanced stoichiometric equations, the composi-

TABLE 4: Estimation of Particle Size for the Decomposed Nickel Formate Dihydrate Based on the Experimental Data Given in Table 3 and Theoretical Calculations of the Coordination Numbers versus Particle Size

particle radius (Å)	no. atoms in cluster	ave first shell occupation number	ave second shell occupation number	ave third shell occupation number	ave fourth shell occupation number
4	19	6.3	1.9	5.1	1.9
6	79	8.5	3.2	11.5	5.0
8	177	9.1	3.9	14.4	6.6
10	369	9.8	4.4	16.3	7.6
15	1205	10.5	4.9	18.7	9.0
QXAFS data (Table 3, column 3)		8.2	3.7	11.9	5.0

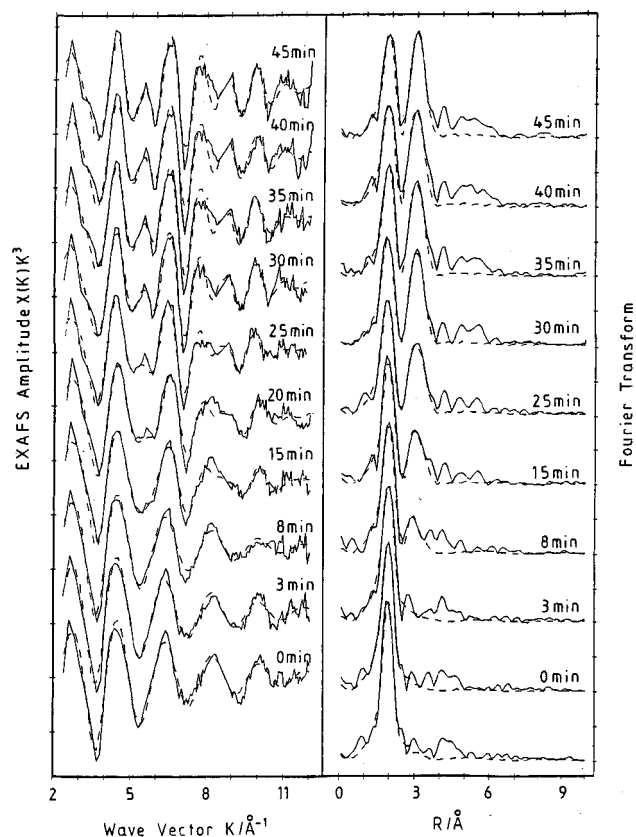


Figure 8. k^3 -weighted time dependent QXAFS data and associated Fourier transforms recorded under isothermal conditions (180 °C) with a fixed integration time of 0.01 s and monochromator speed of 20 mdeg s^{-1} (—) together with simulations based on the parameters listed in Table 5 (---).

TABLE 5: Optimized Parameters Derived from Simulation of EXAFS Data from the Isothermal Decomposition Experiments

time (min)	oxygen			nickel		
	N	R (Å)	2σ (Å ²)	N	R (Å)	2σ (Å ²)
0	4.8	2.01	0.016			
3	4.9	2.02	0.018			
8	4.9	2.02	0.020			
15	4.4	2.01	0.019	1.5	2.96	0.021
20	4.1	2.00	0.018	3.1	2.98	0.024
25	3.7	2.01	0.017	4.7	2.98	0.027
30	3.8	2.01	0.020	6.4	2.99	0.027
35	3.6	2.02	0.017	6.5	2.99	0.027
40	3.9	2.02	0.022	6.3	2.98	0.026
45	3.8	2.02	0.020	6.9	2.99	0.026

tion of each particle at any instant depending in a complex way on its immediate environment. Identification of mechanisms and kinetics for reactions of this type will therefore continue to present a particular challenge.

In general, any parameter that can be related to the fractional extent of a reaction can be used as a kinetic probe if the measurements can be completed on a time scale short relative to the process. No attempt has made to quantify rate constants because of the known sensitivity of the kinetics to factors such as reactant particle subdivision, agglomeration, and ambient atmosphere²⁰ beyond the control of the experiment. Despite this, some qualitative statements are possible. The oxygen coordination number at the beginning of the isothermal experiment (Figure 9) is consistent with partial dehydration having occurred during the temperature elevation phase, implying that this step in the pyrolysis is a rapid one. Similarly, the nonlinear variation in the Ni shell occupation number accords with a

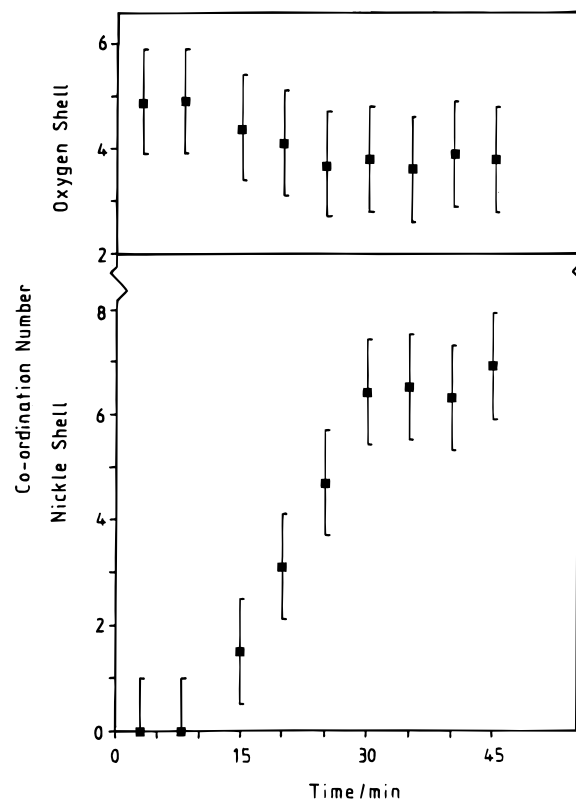


Figure 9. Time dependent evolution of the oxygen (top) and nickel (bottom) shell occupation numbers (estimated uncertainty is ± 1) determined from the isothermal QXAFS experiment. The integration time is 0.01 s, and the monochromator speed is 20 mdeg s^{-1} .

previously reported temperature dependent induction period preceding a brief acceleratory period in the decomposition of the anion, which is subsequently retarded by the accumulation of reaction products.²¹

Conclusions

The application of QXAFS to the structural characterization of materials has been quantitatively demonstrated through a careful examination of the structure, and subsequent thermal decomposition, of nickel formate dihydrate. The study reveals that data acquisition times can be reduced by nearly 2 orders of magnitude when compared with normal (step/count) techniques.

Although currently unable to offer the very high time resolution of dispersive EXAFS,⁵⁴ hardware developments, including high-quality detectors,⁵⁵ are narrowing the gap. Similar experiments carried out on a third generation synchrotron radiation source, such as the ALS (USA), ESRF (Europe) or Spring 8 (Japan), would provide data acquisition times for XANES and EXAFS of ca. 30 and 300 ms, respectively, thus yielding some considerable scope for further developments of the QXAFS method and its application to in situ structurokinetic studies.^{56–60}

Acknowledgment. We thank the CCLRC Daresbury Laboratory for the provision of synchrotron beam time on the SRS, D. Cunningham for recording the DSC data, E. Pantos and N. Harris for their help in implementing the data acquisition software, and EPSRC for the current support of a senior fellowship (K.J.R.).

References and Notes

- (1) Hastings, J. B. In *EXAFS Spectroscopy*; Teo, B. K., Joy, Ed.; Plenum: New York; p 171.
- (2) Hayes, T. M.; Boyce, J. B. *Solid State Phys.* **1982**, *37*, 173.
- (3) Munro, I. H.; Schwentner, N. *Nucl. Instrum. Methods* **1983**, *208*, 819.
- (4) George, G. N.; Bray, R. C.; Cramer, S. P. *Biochem. Soc. Trans.* **1986**, *14*, 651.
- (5) Mills, D. M.; Lewis, A.; Harootunian, A.; Huang, J.; Smith, B. *Science* **1984**, *223*, 811.
- (6) Frahm, R. *Nucl. Instrum. Methods* **1988**, *A270*, 578; *Physica B* **1989**, *158*, 342.
- (7) Lee, P. A.; Citrin, P. H.; Eisenberger, P.; Kincaid, B. M. *Rev. Mod. Phys.* **1981**, *53*, 769.
- (8) Als Nielsen, J.; Grubel, G.; Clausen, B. S. *Nucl. Instrum. Methods* **1995**, *B97*, 522.
- (9) Pantos, E. TOPOGRAPHY; DAG Group, CCLRC Daresbury Laboratory: Warrington, U.K.
- (10) Bhat, H. L.; Clark, S. M.; El Korashy, A.; Roberts, K. J. *J Applied Crystallogr.* **1990**, *23*, 545.
- (11) Gurman, S. J.; Binsted, N.; Ross, I. J. *Phys. C* **1984**, *17*, 143.
- (12) Binsted, N.; Campbell, J. W.; Gurman, S. J.; Stephenson, P. C. *SERC Daresbury Laboratory EXCURV92 Program*; Daresbury Laboratory: Warrington, U.K., 1991.
- (13) Gurman, S. J.; Binsted, N.; Ross, I. J. *Phys. C* **1986**, *19*, 1845.
- (14) von Barth, U.; Hedin, L. *J Phys C* **1972**, *5*, 1629.
- (15) Brillouin, L. *Science and Information Theory*; Academic Press: New York, 1962.
- (16) Moraweck, B.; A. Renouprez, J. *Surf. Sci.* **1981**, *106*, 35.
- (17) Dartigues, J. M.; Chambellan, A.; Corolleur, S.; Gault, F. G.; Renouprez, A. J.; Moraweck, B.; Bosch-Giral, P.; Dalmai-Imelik, G. *Nouv. J. Chim.* **1979**, *3*, 591.
- (18) de Heer, W. A.; Knight, W. D.; Chou, M. Y.; Cohen, M. L. *Solid State Phys.* **1987**, *40*, 93.
- (19) Galwey, A. K.; Brown, M. E. *Proc. R. Irish Acad.* **1977**, *77B*, 465.
- (20) Fox, P. G.; Ehretsmann, J.; Brown, C. E. *J. Catal.* **1971**, *20*, 67.
- (21) Galwey, A. K.; McGinn, M. G.; Brown, M. E. *Proceedings of the 7th International Symposium on Reactivity of Solids*; Chapman and Hall: London, 1972.
- (22) Maiti, G. C.; Kundu, M. L.; Ghosh, S. K.; Banerjee, B. K. *Therm. Anal.* **1974**, *2*, 395.
- (23) Vecher, A. A.; Dalidovich, S. V.; Gusev, E. A. *Thermochim. Acta* **1985**, *89*, 383.
- (24) McCarty, J.; Falconer, J. L.; Madix, R. J. *J. Catal.* **1973**, *30*, 235.
- (25) McCarty, J.; Falconer, J. L.; Madix, R. J. *J. Catal.* **1973**, *31*, 316.
- (26) Falconer, J. L.; Madix, R. J. *Surf. Sci.* **1974**, *46*, 473.
- (27) Falconer, J. L.; Madix, R. J. *Surf. Sci.* **1975**, *48*, 262.
- (28) Falconer, J. L.; Madix, R. J. *J. Catal.* **1977**, *48*, 262.
- (29) Falconer, J. L.; Madix, R. J. *J. Catal.* **1978**, *51*, 47.
- (30) Benziger, J. B.; Madix, R. J. *Surf. Sci.* **1979**, *79*, 394.
- (31) Ying, D. H. S.; Madix, R. J. *J. Catal.* **1980**, *61*, 48.
- (32) Madix, R. J. *Catal. Rev.* **1977**, *15*, 293.
- (33) Barteau, M. A.; Bowker, M.; Madix, R. J. *J. Catal.* **1981**, *67*, 118.
- (34) Benziger, J. B.; Ko, E. I.; Madix, R. J. *J. Catal.* **1979**, *58*, 149.
- (35) McCarty, J.; Madix, R. J. *J. Catal.* **1975**, *38*, 402.
- (36) McCarty, J.; Madix, R. J. *Surf. Sci.* **1976**, *54*, 210.
- (37) Johnson, S. W.; Madix, R. *Surf. Sci.* **1977**, *66*, 189.
- (38) Iglesia, E.; Boudart, M. *J. Catal.* **1984**, *88*, 325.
- (39) Krogmann, K.; Mattes, P. Z. *Crystallogr.* **1963**, *118*, 291.
- (40) Montgomery, H.; Lingafelter, E. C. *Acta Crystallogr.* **1964**, *17*, 1481.
- (41) Pfluger, C. E.; Burke, T. S.; Bednowitz, A. L. *J. Cryst. Mol. Struct.* **1973**, *3*, 181.
- (42) Mounts, R. D.; Fernando, Q. *Acta Crystallogr.* **1974**, *30*, 542.
- (43) Garner, W. E. *Chemistry of the Solid State*; Butterworths Scientific Publications: London, 1955.
- (44) Davis, R. J.; Landry, S. M.; Horsley, J. A.; Boudart, M. *Phys. Rev.* **1989**, *B39*, 10580.
- (45) Shaw, E. A.; Gauntlett, T.; Oldman, R. J.; Dent, A. *Catal. Today* **1991**, *9*, 197.
- (46) Couves, J. W.; Thomas, J. M.; Waller, D.; Jones, R. H.; Dent, A. J.; Derbyshire, G. E.; Greaves, G. N. *Nature* **1991**, *354*, 465.
- (47) Hansen, L. B.; Stoltz, P.; Norskov, J. K.; Clausen, B. S.; Niemann, W. *Phys. Rev. Lett.* **1990**, *64*, 3155.
- (48) Eisenberger, P.; Brown, G. S. *Solid State Commun.* **1979**, *29*, 481.
- (49) Williamson, G. K.; Hall, W. H. *Acta Metall.* **1953**, *1*, 22.
- (50) Flanagan, T. B.; Simons, J. W.; Fichte, P. M. *J. Chem. Soc., Chem Commun.* **1971**, 370.
- (51) Joyner, R. W.; Martin, K. J.; Meecham, P. J. *Phys.* **1987**, *C20*, 4005.
- (52) Sasaki, S.; Fujino, K.; Takeuchi, Y. *Proc. Jpn. Acad.* **1979**, *43*, 55.
- (53) Arkhangel'skil, I. V.; Komissorova, L. N.; Falikman, V. R. *Coord. Khim.* **1977**, *3*, 385.
- (54) Flank, A. M.; Fontaine, A.; Jucha, A.; Lemonnier, M.; Raoux, D.; Williams, C. *Nucl. Instrum. Methods* **1983**, *208*, 651.
- (55) Farrow, R.; Derbyshire, G. E.; Dobson, B. R.; Dent, A. J.; Bogg, D.; Headspith, J.; Lawton, R.; Martini, M.; Buxton, K.; Trammel, R. *Physica B* **1995**, *209*, 256.
- (56) Roberts, K. J.; Robinson, J.; Davies, T. W.; Hooper, R. M. *Jpn. J. Appl. Phys.* **1993**, *32* (2), 652.
- (57) Bhat, H. L.; Roberts, K. J.; Sacchi, M. *J. Phys.: Condens. Matter* **1990**, *2*, 8557.
- (58) Herron, M. E.; Walsh, F. C.; Doyle, S. E.; Pizzini, S.; Roberts, K. J.; Robinson, J.; Hards, G. J. *Electroanal. Chem.* **1992**, *324*, 234.
- (59) Hastie, G. P.; Johnstone, J.; Roberts, K. J.; Fischer, D. *J. Chem. Soc., Faraday Trans.* **1996**, *92*, 783.
- (60) Roberts, K. J.; Adams, D. SERC Daresbury Laboratory Technical Memorandum DL/SCI/TM97E; Daresbury Laboratory: Warrington, U.K., 1993.

JP961488M